IET Power Electronics

Research Article

IET Journals
The Institution of Engineering and Technology

Single-magnetic equaliser without any sensors for series-connected battery strings

ISSN 1755-4535
Received on 4th January 2019
Revised 19th April 2019
Accepted on 16th May 2019
E-First on 11th July 2019
doi: 10.1049/iet-pel.2019.0021
www.ietdl.org

Fulin Liu[1], Runmin Zou[1], Mei Su[1], Yao Sun[1], Yonglu Liu[1], Xing Li[2], Hui Wang[1], Guo Xu[1] ✉

[1]School of Automation, Central South University, Minzhu Building, Changsha, People's Republic of China
[2]Department of Electrical and Electronic Engineering, Hunan University, Changsha, People's Republic of China
✉ *E-mail: xuguocsu@csu.edu.cn*

Abstract: This study proposes an automatic cell-to-cell equaliser to balance the battery voltages in series-connected battery strings. In the proposed equaliser, each cell needs only one MOSFET, and the adjacent cells share the transformer winding. The voltage balance is automatically realised by using a pair of complementary control signals with a fixed duty cycle. What's more, no sensing circuit is required. Consequently, the proposed equaliser is cost-effective and easy-to-realise. The circuit topology and operating principles are firstly presented. Then the voltage balance analysis is given in detail. Moreover, a design guide is also given by considering four lithium-ion cells. Finally, the validity of the proposed equaliser is verified by experimental results.

1 Introduction

Lithium-ion batteries have been one of the most widespread rechargeable batteries due to the advantages of low self-discharge rate, high energy density, high cell voltage, and no memory effect [1, 2]. To meet the requirements of high voltage and large capacity, a large number of lithium-ion battery cells are connected in series and parallel to form a battery pack [3–5]. However, the manufacturing tolerances and environment could lead to differences in the capacities and internal resistances between battery cells. What's worse, the inconsistency will be expanded with the repetitive charging and discharging. Once any cell reaches the charging/discharging cut-off voltage, the whole battery pack stops working, which makes other cells underutilised [6]. Therefore, a battery equaliser is required to make the best use of lithium-ion battery cells.

Many equalisation schemes have been proposed in the last few years [7–9]. They can be classified into two types: passive and active balancing methods. The former [10] is based on energy dissipation, which utilises the dissipative element to drain excess energy in higher voltage cells. The highlights of this method are low cost and simple control. However, the available capacity of the battery pack is reduced as the excess energy is dissipative.

As for the active balancing method, the excess energy from higher voltage cells is transferred to lower ones. Hence, a more efficient and rapid balance can be realised. Generally, passive elements such as inductors [11–15], capacitors [16–20], transformers [21–29], and their combinations [30, 31] are required to achieve the energy transfer. More information on the mathematical model and control of battery equalisation systems is summarised in [32–34].

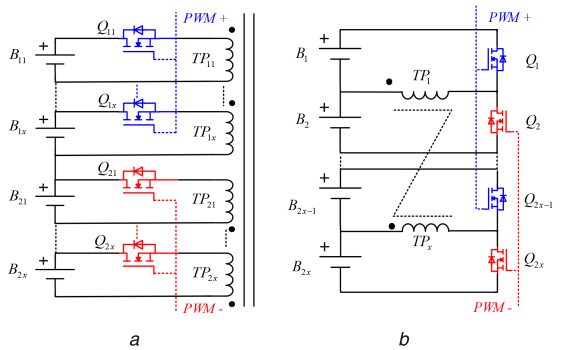

Fig. 1 *Battery equalisers using a multi-winding transformer*
(a) Equaliser based on forward–flyback conversion [29],
(b) Proposed equaliser

It is a good way to balance the energy of batteries by using the state-of-charge (SOC). The model-based estimation methods, which used the equivalent circuit model, are widely applied to obtain the SOC of batteries [15, 35]. However, the number of sensors increases with the increasing number of cells, which raises the cost and the control complexity. Simply balancing by voltage is commonly adopted, and the results are acceptable [18–20, 27–29].

To reduce the cost and control complexity, some equalisers with no voltage sensors are developed. Lim *et al.* [27] propose a modularised equaliser based on a flyback converter. The magnetising energy of the multi-winding transformer is utilised to equalise cells, which reduces the size and cost. However, the equalisation speed and battery life are reduced as the equaliser transmits energy from cells into groups. What's worse, the application is limited to the case with one or two battery modules. Li *et al.* [28] propose a simple circuit of battery equaliser using a symmetrical multi-winding transformer. Each cell is configured with only one MOSFET and one winding. Only one control signal is required for all the MOSFETs, and energy can be directly transferred from higher voltage cells to lower ones. The disadvantage is that the additional circuit is used to achieve demagnetising and modular structure. As shown in Fig. 1*a*, Shang *et al.* [29] propose a battery equaliser based on the forward-flyback converter. All MOSFETs are controlled by one pair of complementary pulse-width modulation (PWM) signals, and the magnetic energy stored in the transformer is automatically reset. However, the energy stored in the leakage inductance is wasted when the switches are turned off.

To further reduce the size and cost, this paper proposes an automatic equaliser with reduced transformer windings and without sensing circuit. It is an improvement of the work in [29]. The used windings are reduced by sharing one winding between two adjacent cells. Moreover, all MOSFETs are driven by a pair of complementary control signals with a fixed duty ratio. Then, energy can be directly transferred from higher voltage cells to lower ones to achieve voltage balance. Low cost, small size, simple control, and wide applicability are the main advantages of the proposed equaliser. The rest of the paper is organised as follows: the introduction and voltage balancing principle of the topology are described in Section 2. Section 3 demonstrates the design guide of an equaliser for four cells and shows experimental results. A

$$\begin{cases} i_1(t) = \mathrm{e}^{-(R(t-t_1)/(L+2L_{\mathrm{M}}))}\dfrac{E_2+E_4+Ri_1(t_1)+Ri_2(t_1)}{2R} + \mathrm{e}^{-(R(t-t_1)/L)}\dfrac{E_2-E_4+Ri_1(t_1)-Ri_2(t_1)}{2R} - \dfrac{E_2}{R} \\ i_2(t) = \mathrm{e}^{-(R(t-t_1)/(L+2L_{\mathrm{M}}))}\dfrac{E_2+E_4+Ri_1(t_1)+Ri_2(t_1)}{2R} - \mathrm{e}^{-(R(t-t_1)/L)}\dfrac{E_2-E_4+Ri_1(t_1)-Ri_2(t_1)}{2R} - \dfrac{E_4}{R} \end{cases} \quad (7)$$

comparative study is provided in Section 4, followed by the conclusion in Section 5.

2 Proposed equaliser

2.1 Operation principles

The proposed equaliser is shown in Fig. 1*b*. The battery string includes x groups, and each group consists of the adjacent two cells, two MOSFETs and one shared winding. The two MOSFETs in each group are driven by a pair of complementary signals, i.e. all the upper MOSFETs are driven by PWM+, and the others are driven by the complementary signal PWM−.

The detailed analysis of the equaliser for four cells is presented as follows, and other cases can be similarly analysed. For the convenience of analysis, the following assumptions are given:

(i) The battery string comprised of two groups is taken as an example, and the circuit model is shown in Fig. 2. The windings in each group have the same turn number. R represents the equivalent resistance. L and L_{M} represent the leakage and magnetising inductance of the multi-winding transformer, respectively.
(ii) In each group, the upper MOSFET is driven by PWM+, and the other is driven by PWM−. All of the duty ratios are set to be 50%.
(iii) E_i ($i = 1, 2, 3,$ and 4.) represents the battery voltages of B_i. The initial voltages of battery cells satisfy $E_1 > E_2 > E_3 > E_4$. And the terminal voltages of battery cells are constant during a switching period.
(iv) i_1 and i_2 represent the currents of leakage inductance, i_0 represents the load current of the battery string.

From Fig. 2, the equaliser has two switching states during a switching period, i.e. State I and State II. The relevant equivalent circuits are shown in Fig. 3.

State I (t_0–t_1): In this state, switches Q_1 and Q_3 are turned on and switches Q_2 and Q_4 are turned off. Its equivalent circuit model is shown in Fig. 3*a*.

According to Fig. 3*a*, the following differential equations are obtained as:

$$\begin{cases} L\dfrac{\mathrm{d}i_1(t)}{\mathrm{d}t} = E_1 - Ri_1(t) - L_{\mathrm{M}}\dfrac{\mathrm{d}[i_1(t)+i_2(t)]}{\mathrm{d}t} \\ L\dfrac{\mathrm{d}i_2(t)}{\mathrm{d}t} = E_3 - Ri_2(t) - L_{\mathrm{M}}\dfrac{\mathrm{d}[i_1(t)+i_2(t)]}{\mathrm{d}t} \end{cases} \quad (1)$$

Suppose the initial conditions are

$$\begin{cases} i_1(t)\big|_{t=t_0} = i_1(t_0) \\ i_2(t)\big|_{t=t_0} = i_2(t_0) \end{cases} \quad (2)$$

Then, the solutions of (1) are expressed as (see (3)) . Hence, at the end of state I

$$\begin{cases} i_1(t)\big|_{t=t_1} = \dfrac{E_1}{R} - A\dfrac{E_1+E_3-Ri_1(t_0)-Ri_2(t_0)}{2R} - B\dfrac{E_1-E_3-Ri_1(t_0)+Ri_2(t_0)}{2R} \\ i_2(t)\big|_{t=t_1} = \dfrac{E_3}{R} - A\dfrac{E_1+E_3-Ri_1(t_0)-Ri_2(t_0)}{2R} + B\dfrac{E_1-E_3-Ri_1(t_0)+Ri_2(t_0)}{2R} \end{cases} \quad (4)$$

where $A = \mathrm{e}^{-RT/2(L+2L_{\mathrm{M}})}$, $B = \mathrm{e}^{-RT/2L}$, $t_1 = t_0 + T/2$, and T is the switching period.

State II (t_1–t_2 (T)): In this state, switches Q_2 and Q_4 are turned on and switches Q_1 and Q_3 are turned off. The equivalent circuit model is shown in Fig. 3*b*.

According to Fig. 3*b*, the differential equations of the circuit are formulated as follows:

$$\begin{cases} L\dfrac{\mathrm{d}i_1(t)}{\mathrm{d}t} = -E_2 - Ri_1(t) - L_M\dfrac{\mathrm{d}[i_1(t)+i_2(t)]}{\mathrm{d}t} \\ L\dfrac{\mathrm{d}i_2(t)}{\mathrm{d}t} = -E_4 - Ri_2(t) - L_M\dfrac{\mathrm{d}[i_1(t)+i_2(t)]}{\mathrm{d}t} \end{cases} \quad (5)$$

Assume the initial conditions are

$$\begin{cases} i_1(t)\big|_{t=t_1} = i_1(t_1) \\ i_2(t)\big|_{t=t_1} = i_2(t_1) \end{cases} \quad (6)$$

Then, the solution of formulas (5) is expressed as (see (7)) . Hence, at the end of state II

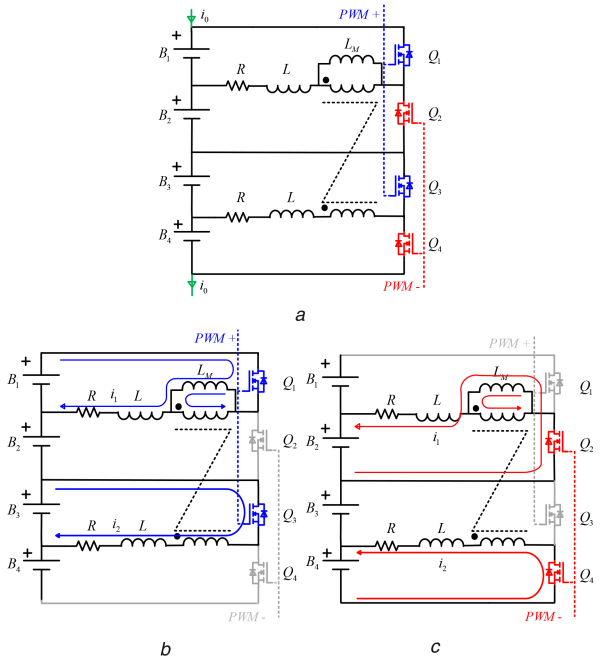

Fig. 2 *Circuit model and operating states of the proposed equaliser*
(a) Model,
(b) State I,
(c) State II

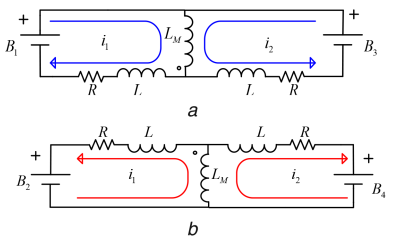

Fig. 3 *Equivalent circuit model*
(a) State I,
(b) State II

$$\begin{cases} i_1(t) = \dfrac{E_1}{R} - \mathrm{e}^{-(R(t-t_0)/(L+2L_{\mathrm{M}}))}\dfrac{E_1+E_3-Ri_1(t_0)-Ri_2(t_0)}{2R} - \mathrm{e}^{-(R(t-t_0)/L)}\dfrac{E_1-E_3-Ri_1(t_0)+Ri_2(t_0)}{2R} \\ i_2(t) = \dfrac{E_3}{R} - \mathrm{e}^{-(R(t-t_0)/(L+2L_{\mathrm{M}}))}\dfrac{E_1+E_3-Ri_1(t_0)-Ri_2(t_0)}{2R} + \mathrm{e}^{-(R(t-t_0)/L)}\dfrac{E_1-E_3-Ri_1(t_0)+Ri_2(t_0)}{2R} \end{cases} \quad (3)$$

$$i_1(t)=\begin{cases}\frac{E_1}{R}-\mathrm{e}^{-(R/(L+2L_M))(t-t_0)}\frac{E_1+E_2+E_3+E_4}{2R(1+A)}-\mathrm{e}^{-(R/L)(t-t_0)}\frac{E_1+E_2-E_3-E_4}{2R(1+B)}, & (t_0\le t<t_1)\\ -\frac{E_2}{R}+\mathrm{e}^{-(R/(L+2L_M))(t-t_1)}\frac{E_1+E_2+E_3+E_4}{2R(1+A)}+\mathrm{e}^{-(R/L)(t-t_1)}\frac{E_1+E_2-E_3-E_4}{2R(1+B)}, & (t_1\le t\le t_2)\end{cases} \tag{9}$$

$$i_2(t)=\begin{cases}\frac{E_3}{R}-\mathrm{e}^{-(R/(L+2L_M))(t-t_0)}\frac{E_1+E_2+E_3+E_4}{2R(1+A)}+\mathrm{e}^{-(R/L)(t-t_0)}\frac{E_1+E_2-E_3-E_4}{2R(1+B)}, & (t_0\le t<t_1)\\ -\frac{E_4}{R}+\mathrm{e}^{-(R/(L+2L_M))(t-t_1)}\frac{E_1+E_2+E_3+E_4}{2R(1+A)}-\mathrm{e}^{-(R/L)(t-t_1)}\frac{E_1+E_2-E_3-E_4}{2R(1+B)}, & (t_1\le t\le t_2)\end{cases}. \tag{10}$$

$$\begin{cases}i_1(t)\big|_{t=t_2}=-\frac{E_2}{R}+A\frac{E_2+E_4+Ri_1(t_1)+Ri_2(t_1)}{2R}+B\frac{E_2-E_4+Ri_1(t_1)-Ri_2(t_1)}{2R}\\ i_2(t)\big|_{t=t_2}=-\frac{E_4}{R}+A\frac{E_2+E_4+Ri_1(t_1)+Ri_2(t_1)}{2R}-B\frac{E_2-E_4+Ri_1(t_1)-Ri_2(t_1)}{2R}\end{cases} \tag{8}$$

where $A=\mathrm{e}^{-RT/2(L+2L_M)}$, $B=\mathrm{e}^{-RT/2L}$, $t_1=t_0+T/2$, and T is the switching period.

Compared with the voltages of battery cells, the current could quickly enter into the steady state. Thus, it is reasonable to assume that $i_1(t_2)=i_1(t_0)$, $i_2(t_2)=i_2(t_0)$. From (3), (4), (7), and (8), currents i_1 and i_2 are obtained

(see (9))

(see (10))

According to the direction of the current in Fig. 3, during $t_0\le t<t_1$, $i_1(t)$ and $i_2(t)$ are assumed to be the discharging current of B_1 and B_3. While during $t_1\le t\le t_2$, $i_1(t)$ and $i_2(t)$ are assumed to be the charging current of B_2 and B_4.

2.2 Voltage balance analysis

From Fig. 4, the average transmission power of the four cells over each switching period could be expressed as follows:

$$\begin{cases}P_1=\frac{E_1}{T}\int_{t_0}^{t_1}i_1(t)\,\mathrm{d}t\\ P_2=-\frac{E_2}{T}\int_{t_1}^{t_2}i_1(t)\,\mathrm{d}t\\ P_3=\frac{E_3}{T}\int_{t_0}^{t_1}i_2(t)\,\mathrm{d}t\\ P_4=-\frac{E_4}{T}\int_{t_1}^{t_2}i_2(t)\,\mathrm{d}t\end{cases}. \tag{11}$$

According to (9) and (10), (11) is rewritten as

$$\begin{cases}P_1=aE_1^2-bE_1-cE_1\\ P_2=aE_2^2-bE_2-cE_2\\ P_3=aE_3^2-bE_3+cE_3\\ P_4=aE_4^2-bE_4+cE_4\end{cases} \tag{12}$$

where

$$c=\frac{(E_1+E_2-E_3-E_4)L(1-B)}{2TR^2(1+B)},$$
$$b=\frac{(E_1+E_2+E_3+E_4)(L+2L_M)(1-A)}{2TR^2(1+A)},\quad a=\frac{1}{2R}.$$

If $P_i>0$ ($i=1, 2, 3, 4$), the cell releases energy; otherwise, it stores energy.

In the following analysis, the battery cell is replaced by an ideal voltage source U_o, a resistor R_o and a capacitor C [36]. U_o represents the initial voltage of the battery, R_o is the internal resistor, and C represents the A–H capacity of the cell. The terminal voltage of a battery is obtained as

$$E_i=U_o+U_i+R_o(i_0+i_{bi}) \tag{13}$$

where U_i ($i=1$, 2, 3, and 4) is the voltage of the capacitor, i_0 is the load current of the battery string and is taken as a constant in the following, i_{bi} is the equalisation current of the battery cell.

If the voltage differences of the capacitors converge to zero, the balance of cells will be achieved. The differential equations of the circuit are formulated as follows:

$$C\frac{\mathrm{d}U_1}{\mathrm{d}t}=i_0-\frac{P_1}{E_1}=i_0-(aE_1-b-c) \tag{14a}$$

$$C\frac{\mathrm{d}U_2}{\mathrm{d}t}=i_0-\frac{P_2}{E_2}=i_0-(aE_2-b-c) \tag{14b}$$

$$C\frac{\mathrm{d}U_3}{\mathrm{d}t}=i_0-\frac{P_3}{E_3}=i_0-(aE_3-b+c) \tag{14c}$$

$$C\frac{\mathrm{d}U_4}{\mathrm{d}t}=i_0-\frac{P_4}{E_4}=i_0-(aE_4-b+c). \tag{14d}$$

Subtracting (14b) from (14a) leads to

$$C\frac{\mathrm{d}U_{12}}{\mathrm{d}t}=-aE_{12} \tag{15}$$

where $U_{12}=U_1-U_2$, $E_{12}=E_1-E_2$. According to (13) and (15) is rewritten as

$$\frac{\mathrm{d}U_{12}}{\mathrm{d}t}=\frac{a}{C(aR_0-1)}U_{12} \tag{16}$$

where $a=(1/2R)$. As $(a/(aR_0-1))=(1/(R_0-2R))<0$, U_{12} will converge to zero. Therefore, the balance of B_1 and B_2 will be achieved.

Subtracting (14c) from (14a) and subtracting (14d) from (14b) lead to

$$\begin{cases}C\frac{\mathrm{d}U_{13}}{\mathrm{d}t}=-aE_{13}+2c\\ C\frac{\mathrm{d}U_{24}}{\mathrm{d}t}=-aE_{24}+2c\end{cases} \tag{17}$$

where $U_{13}=U_1-U_3$, $U_{24}=U_2-U_4$, $E_{13}=E_1-E_3$, $E_{24}=E_2-E_4$. According to (13) and (17) are rewritten as

$$\begin{cases}\frac{\mathrm{d}U_{13}}{\mathrm{d}t}=mU_{13}+nU_{24}\\ \frac{\mathrm{d}U_{24}}{\mathrm{d}t}=nU_{13}+mU_{24}\end{cases} \tag{18}$$

where

$$m=\frac{k+a(aR_0-2kR_0-1)}{(aR_0-1)(aR_0-2kR_0-1)C},$$
$$n=\frac{k}{(aR_0-1)(aR_0-2kR_0-1)C},\quad k=\frac{L(1-B)}{TR^2(1+B)}.$$

As $m+n<0$ and $m-n<0$ (see Appendix for the detailed analysis), U_{13} and U_{24} will also converge to zero.

According to the analysis above, effective balancing among all cells is automatically achieved. What's more, the state of the battery string (charging, discharging, or rest) and the internal resistor do not affect the work of the equaliser.

Since the value of the leakage inductance is very small, the voltage equalisation speed mainly depends on the time constant R and C. Thus, R is a critical parameter in controlling equalisation speed.

Meanwhile, the effect of R on power loss is discussed as follows. From (12), the power loss of R and conduction losses of MOSFETs are obtained

$$P_{\text{loss}} = a(E_1^2 + E_2^2 + E_3^2 + E_4^2) - e \tag{19}$$

where $a = (1/2R)$ and $e = \left(\left((E_1 + E_2 + E_3 + E_4)^2(L + 2L_{\text{M}})(1 - A)\right)/2TR^2(1 + A)\right)$.

The switching losses of MOSFETs can be obtained by

$$P_{\text{s\_loss}} = \frac{f}{T}\int_0^T \frac{1}{2} i_m v_{\text{ds}}(t_{\text{off}} + t_{\text{on}}) + \frac{1}{2} C_{\text{oss}} v_{\text{ds}}^2 \, \text{d}t \,. \tag{20}$$

According to (12) and (19), (20), the power loss rate is obtained

$$\eta_{\text{loss}} = \frac{P_{\text{loss}} + P_{\text{s\_loss}}}{P_{\text{out}}} \tag{21}$$

where P_{out} is the total power of cells which release energy. The power loss rates with respect to P_{out} and R are shown in Fig. 5 by using parameters in Table 1. Clearly, the power loss rates decrease with the decrease of R.

In summary, R should be set as low as possible to improve the equalisation speed and balancing efficiency.

2.3 Expanded study

The equaliser can be used for battery strings with a different number of cells.

As for the case of odd cells, the leakage inductor of the independent winding is not utilised anymore. And the energy stored in the leakage inductor dissipates when the states change. Taking three cells as an example, as shown in Fig. 6*a*, i_2 drops to zero and i_1 grows up to i_{M} when Q_1 and Q_3 are turned off, and Q_2 is turned on.

For operation principles, a similar analysis can be applied. The initial conditions are expressed as

$$\begin{cases} i_1(t)\big|_{t=t_0} = i_1(t_0) \\ i_2(t)\big|_{t=t_0} = 0 \end{cases} \tag{22}$$

$$i_1(t)\big|_{t=t_1} = i_{\text{M}}(t_1) = i_1(t_1) + i_2(t_1) \,. \tag{23}$$

Then, the currents i_1 and i_2 can be expressed as

(see (24))

(see (25))

where

$$i_1(t_0) = \frac{-E_2 + \text{e}^{-(RT/2(L+L_{\text{M}}))}[E_1 + E_2 + E_3 - A(E_1 + E_3)]}{R\left(1 - \text{e}^{-(RT/2)((1/(L+L_{\text{M}})) + (1/(L+2L_{\text{M}})))}\right)} \,.$$

The voltage balance analysis is similar to that in Section 2.2, and it will not be repeated here.

Because a transformer cannot balance all the cells in some applications, the modularised method is proposed. As shown in Fig. 6*b*, every module consists of $2x$ cells, $2x$ MOSFETs, and one transformer with x windings and one additional winding TS. When one transformer cannot meet the requirement, the additional windings TS from different modules can be connected to the same polarity in parallel. Likewise, only a pair of complementary control signals are used. Also, the number of cells in each module is $2x$ and it is limited by the maximum balancing current and the maximum magnetising current.

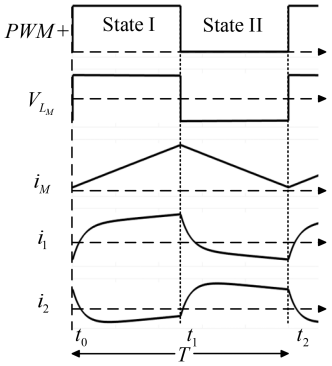

Fig. 4 *Key waveforms of the proposed equaliser*

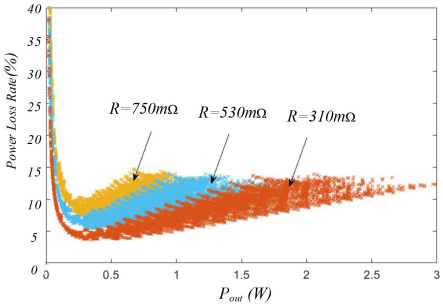

Fig. 5 *Relation curve of η_{loss} versus P_{out} and R*

Table 1 Experimental parameters

Parameters		Value
battery	model	ICR18650-26F
	nominal capacity	2600 mAh
	nominal voltage	3.7 V
	standard charging current	1.35 A
	internal resistance	<100 mΩ
MOSFET	model	IRF3707Z
	on-resistance	9.5 mΩ
transformer	NP_1:NP_2:NS_1	1:1:6
	L_{M}	167 μH
	L	0.3 μH

3 Experimental results

To verify the feasibility of the proposed equaliser, a prototype with four lithium-ion cells connected in series has been built. Fig. 7 shows the implemented prototype and Table 1 lists the main parameters. The control board generates a pair of complementary PWM singles to control the MOSFETs.

3.1 Design consideration

The key design parameters of the equaliser consist of switch frequency f, magnetising inductance L_{M}, the maximum discharging and charging current i_{peak}, the maximum magnetising current i_{Mpeak}, and the equivalent resistance R.

The voltage range of the used battery (ICR18650-26F) is 2.75–4.2 V. Considering the voltage margin, transformer parameters and so on, the voltage range of 3–4 V is used in this paper. To improve the equalisation speed and the balancing efficiency, the voltage difference between the four cells is limited to 0.400 V in the extreme condition. Due to the symmetry structure of the transformer, the desired duty cycle is 50%, the turns ratio is 1:1.

To reduce the hysteresis loss and no-load loss, the ripple current, in any case, is limited to 0.6 A. As the switching frequency

$$i_1(t)=\begin{cases}\dfrac{E_1}{R}-\mathrm{e}^{-(R(t-t_0)/(L+2L_M))}\dfrac{E_1+E_3-Ri_1(t_0)}{2R}-\mathrm{e}^{-(R(t-t_0)/L)}\dfrac{E_1-E_3-Ri_1(t_0)}{2R}, & (t_0\le t<t_1)\\ -\dfrac{E_2}{R}+\mathrm{e}^{-(R(t-t_1)/(L+L_M))}\dfrac{E_2+E_1+E_3-A(E_1+E_3-Ri_1(t_0))}{R}, & (t_1\le t\le t_2)\end{cases} \tag{24}$$

$$i_2(t)=\begin{cases}\dfrac{E_3}{R}-\mathrm{e}^{-(R(t-t_0)/(L+2L_M))}\dfrac{E_1+E_3-Ri_1(t_0)}{2R}+\mathrm{e}^{-(R(t-t_0)/L)}\dfrac{E_1-E_3-Ri_1(t_0)}{2R}, & (t_0\le t<t_1)\\ 0, & (t_1\le t\le t_2)\end{cases} \tag{25}$$

is set to 20 kHz. The magnetising inductance of the multi-winding transformer is obtained as follows:

$$L_M\ge\frac{E_{MAX}}{i_{rip}}\times 0.5\times T=167\,\mu\mathrm{H}. \tag{26}$$

Although a large magnetising inductance can reduce the ripple current in any case, the size will increase. By compromise, the magnetising inductance is selected as 167 µH.

The maximum balancing current i_{peak} of the battery is limited to 1.2 A. From (9), the constraint of the resistance R is expressed as

$$R\ge\frac{E_{MAX}}{i_{peak}}-A\frac{E_{MAX}+3E_{MIN}}{2i_{peak}(1+A)}-B\frac{E_{MAX}-E_{MIN}}{2i_{peak}(1+B)}=0.283\,\Omega. \tag{27}$$

To avoid saturation of the transformer, the maximum magnetising current i_{Mpeak} is limited to 1.6 A. From (9) and (10), the constraint of the resistance R is expressed as

$$R\ge\frac{E_{MAX}+E_{MIN}}{i_{Mpeak}}-A\frac{2E_{MAX}+2E_{MIN}}{i_{Mpeak}(1+A)}=0.305\,\Omega. \tag{28}$$

According to (27) and (28), R is set to be 0.305 Ω.

3.2 Experimental waveforms

Since the design consideration is derived from a theoretical model, the theoretical analysis can be proved through the experimental waveforms.

When the initial values of E_1, E_2, E_3, and E_4 are 4.013, 3.903, 3.702 and 3.608 V, respectively. As shown in Fig. 8*a*, when switches Q_1 and Q_3 are turned on, energy is automatically transferred from B_1 to B_3 and the magnetising inductance. When switches Q_2 and Q_4 are turned on, energy is automatically

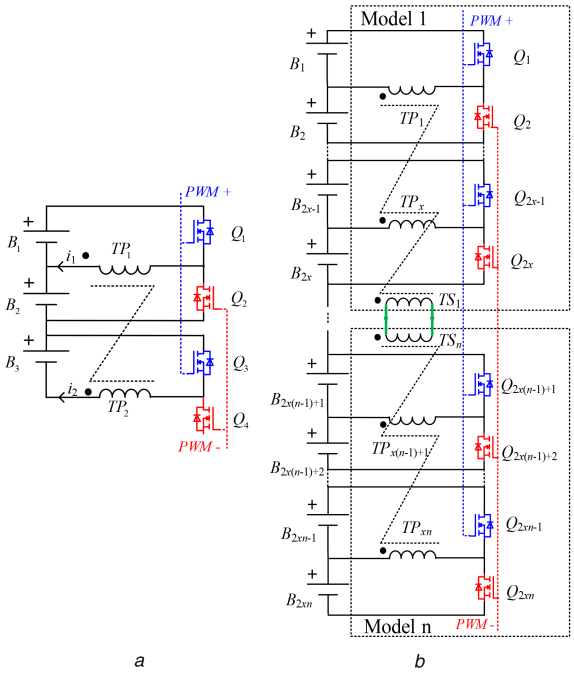

Fig. 6 *Proposed equaliser*
(a) Odd cells,
(b) Modularised structure

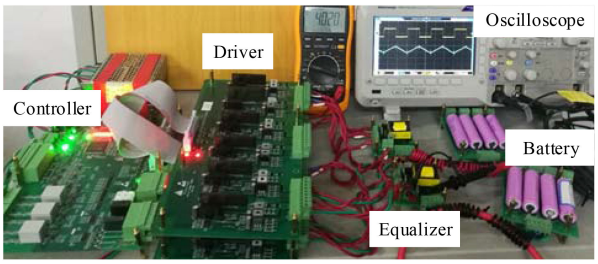

Fig. 7 *Experimental setup*

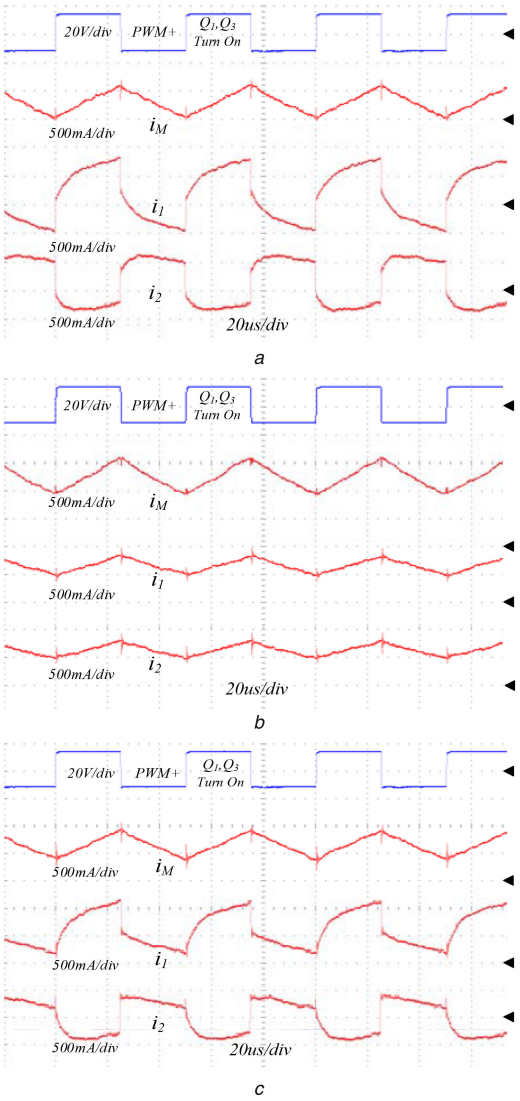

Fig. 8 *Experimental waveforms*
(a) General current,
(b) High magnetising current,
(c) High balancing current

transferred from B_2 and the magnetising inductance to B_4. The average balancing currents flowing out from B_1 and B_2 are ∼310 and 125 mA, and the average balancing currents flowing in B_3 and B_4 are ∼130 and 300 mA. An automatic energy transmission from higher voltage cells to lower ones is achieved. This result agrees with the previous theoretical analysis in Fig. 4.

When the initial values of E_1, E_2, E_3, and E_4 are 4.020, 3.595, 4.016 and 3.609 V, respectively, as shown in Fig. 8*b*, the ripple current is about 0.6 A, and the value of magnetising current is about 1.6 A ($i_M = i_1 + i_2$). The average f balancing current flowing in B_2 and B_4 from B_1 and B_3 is ∼325 mA.

When the initial values of E_1, E_2, E_3, and E_4 are 3.995, 3.598, 3.612 and 3.602 V, respectively, as shown in Fig. 8*c*, the ripple current is about 0.55 A, and the value of balancing current is about 1.15 A. These results agree well with the design consideration and the theoretical analysis.

3.3 Balancing results

In this section, all the values of cell voltages are measured by a multimeter. Fig. 9 shows the equalisation results with different initial voltages. The voltage equalisation is achieved in the two imbalanced situations. And the maximum voltage difference is reduced from 401 to 15 mV. This proves that the proposed

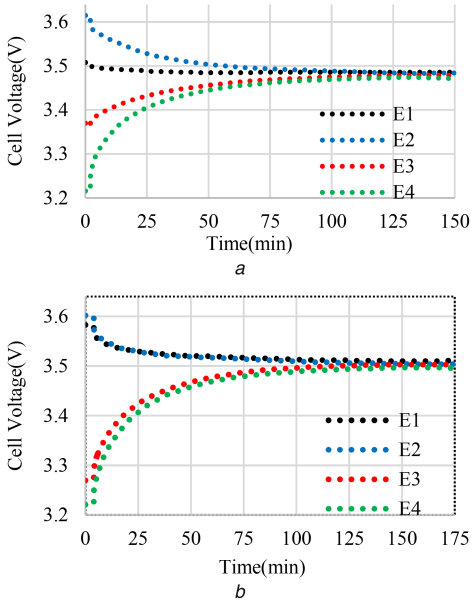

Fig. 9 *Experimental results for four battery cells with different initial voltages*
(a) Case I,
(b) Case II

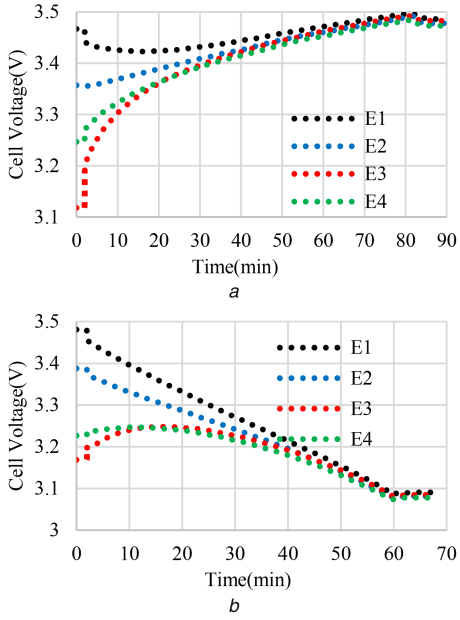

Fig. 10 *Dynamic equalisation results for four battery cells*
(a) Charging,
(b) Discharging

equaliser can be applied to the imbalanced situations with different initial voltages.

The dynamic balancing results are shown in Fig. 10, which can prove the validity of the proposed equaliser. As shown in Fig. 10*a*, the battery string is charged with the constant current, and the maximum voltage difference is reduced from 349 to 14 mV. As shown in Fig. 10*b*, the battery string is discharged with the constant load, and the maximum voltage difference is reduced from 312 to 13 mV. It can be observed that the proposed equaliser achieves voltage equalisation regardless of the state of the battery string (charging, discharging, or rest).

Fig. 11 shows the equalisation results for battery strings with a different number of cells. And the minimum voltage difference is reduced to 14 mV. Although the equaliser can be applied to the equalisation between odd number cells or non-adjacent cells, the advantage of the effective use of leakage inductance is lost. Compared with [29], only the number of windings is reduced.

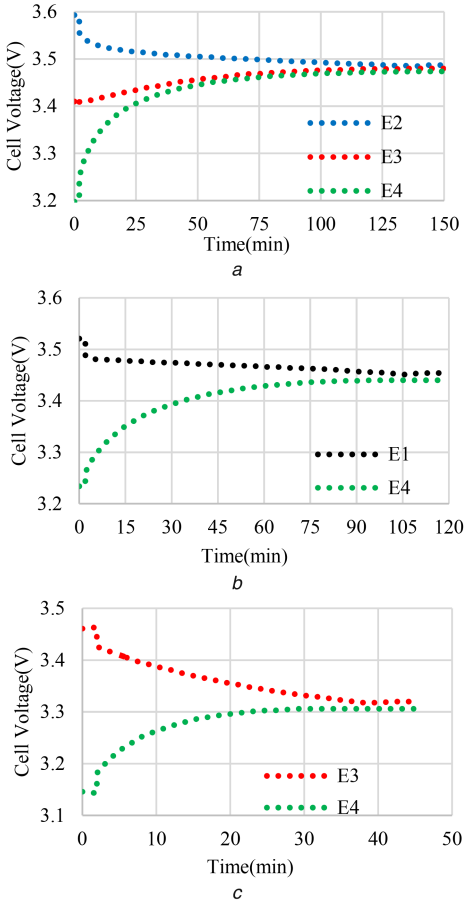

Fig. 11 *Experimental results for battery strings with a different number of cells*

(a) Equalisation for B_2, B_3, and B_4,

(b) Equalisation for B_1 and B_4,

(c) Equalisation for B_3 and B_4

Fig. 12 shows the modularised equalisation result for eight battery cells. The equalisation between modules is easily achieved by connecting the winding NS_1 in parallel. The initial cell voltages are 3.344, 3.469, 3.553, 3.634, 3.476, 3.385, 3.295, and 3.147 V, respectively, and the maximum voltage difference is reduced from 498 to 13 mV. This validity of the proposed modularised equaliser is verified.

Finally, balancing efficiency is measured through experiments. The efficiency concerning the transmission power P_{out} is shown in Fig. 13. P_{out} is the total power of cells, which release energy. The efficiency is the ratio of the total power of cells, which receive energy and P_{out}. And the power used for the calculation is obtained from average current and cells voltage during five switching cycles. Since the conditions (the values of E_1, E_2, E_3 and E_4) are different and changing, the results are measured by balancing four cells in five different conditions. Compared with the calculated loss of Fig. 5, the total loss increases, which could be caused by magnetic loss. These results show that the proposed equaliser can work with high efficiency at different conditions, and achieves the highest efficiency of 90.2%.

4 Comparative study

Compared with the conventional equalisers, the advantage of the proposed equaliser is that no sensing circuit is required. This advantage will reduce the system complexity, the cost and the size. Detailed comparisons between different equalisers have been presented in [29]. To avoid repetition, the comparison is only carried out between the proposed method and the one proposed in [29].

Table 2 shows the comparison results in terms of components, balancing mode, cost, and size. In both of them, only one MOSFET

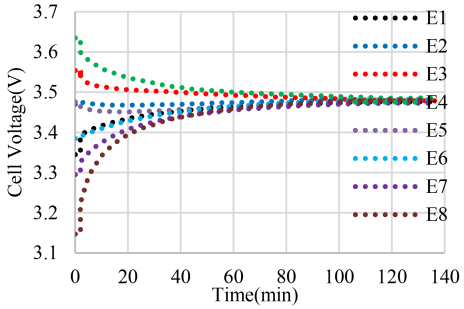

Fig. 12 *Modularised equalisation result for eight battery cells, which are divided into two modularisations*

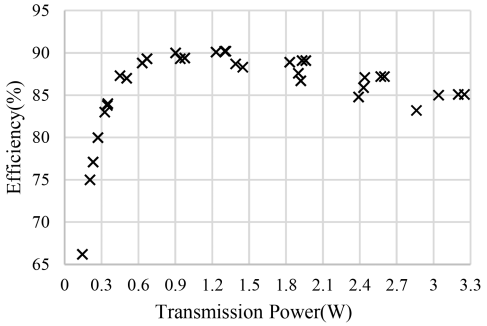

Fig. 13 *Measured balancing efficiency concerning the transmission power P_{out}*

is required for each cell, one pair of complementary control signals are employed for all MOSFETs, and energy is automatically and directly delivered from high-voltage cells to low-voltage ones without using voltage sensors. Thus, low cost, small size, and simple control are the main advantages of them. Compared with the proposed equaliser in [29], the proposed topology has the following improved features:

(i) The adjacent two cells share a winding of the transformer. Therefore, the number of windings is cut in half compared with the method proposed in [29], resulting in smaller circuit size and lower cost, especially in the case of long series-connected battery strings.
(ii) For the forward-flyback equaliser [29], the leakage inductance current drops to zero when the switches are turned off. Consequently, the energy stored in the leakage inductance is wasted and the stress of the device increases. However, that is avoided in the proposed topology.
(iii) The leakage inductance in the equaliser [29] should be set as small as possible to reduce the negative influence, which increases the design difficulty of the transformer. For the proposed equaliser, the issue is avoided and the cost is reduced.

5 Conclusion

An improved automatic battery equaliser with a reduced number of transformer windings is proposed in this paper. Its highlights are low cost and simple control. The winding of the transformer is shared between the two adjacent cells, and the leakage inductance is effectively utilised. Also, all MOSFETs are driven by a pair of complementary control signals, and energy can be directly transferred from higher voltage cells to lower ones without using sensing circuits. Moreover, the number of the cells and the state of the battery string do not affect the work of the equaliser, leading to wide applicability. The experimental platform has been set up to verify the theoretical analysis. In short, the proposed equaliser can be a good candidate for long series-connected battery strings, especially for the case with a low voltage difference between cells.

Table 2 Comparison between different equalisers

Equalisers	Number of MOSFETs	Number of windings	Leakage inductance	Balancing mode	Cost	Size
Shang *et al*. [29]	*n*	*n*	no utilisation	cell-to-cell	high	large
proposed equaliser	*n*	*n*/2	utilisation	cell-to-cell	low	small

Note: *n* is the number of cells in the battery string.

6 Acknowledgments

This work is supported in part by National Key R&D Program of China under grant no. 2018YFB0606005, Natural Science Foundation of China under grant no. 61573384 and grant no. 51807206, the Key Technology R&D Program of Hunan Province of China under grant no. 2018SK2140 and the Fundamental Research Funds in the Central South University under grant no. 2018zzts529.

7 References

[1] Hwang, J.C., Chen, J.C., Pan, J.S., *et al.*: 'Measurement method for online battery early faults precaution in uninterrupted power supply system', *IET Electr. Power Appl.*, 2011, **5**, (3), pp. 267–274

[2] Jaguemont, J., Boulon, L., Venet, P., *et al.*: 'Lithium-ion battery aging experiments at subzero temperatures and model development for capacity fade estimation', *IEEE Trans. Veh. Technol.*, 2016, **65**, (6), pp. 4328–4343

[3] Lukic, S.M., Cao, J., Bansal, R.C., *et al.*: 'Energy storage systems for automotive applications', *IEEE Trans. Ind. Electron.*, 2008, **55**, (6), pp. 2258–2267

[4] Cao, J., Emadi, A.: 'A new battery/ultracapacitor hybrid energy storage system for electric hybrid and plug-in hybrid electric vehicles', *IEEE Trans. Power Electron.*, 2012, **27**, (1), pp. 122–132

[5] Huang, W., Abu Qahouq, J.A.: 'Energy sharing control scheme for state-of-charge balancing of distributed battery energy storage system', *IEEE Trans. Ind. Electron.*, 2015, **62**, (5), pp. 2764–2776

[6] Affanni, A., Bellini, A., Franceschini, G., *et al.*: 'Battery choice and management for new-generation electric vehicles', *IEEE Trans. Ind. Electron.*, 2005, **52**, (5), pp. 1343–1349

[7] Cao, J., Schofield, N., Emadi, A.: 'Battery balancing methods: a comprehensive review'. Proc. Vehicle Power Propulsion Conf., Harbin, China, 2008, pp. 1–6

[8] Daowd, M., Omar, N., Van den Bossche, P., *et al.*: 'Passive and active battery balancing comparison based on MATLAB simulation'. Proc. IEEE Vehicle Power Propulsion Conf., Chicago, IL, USA, 6–9 September 2011, pp. 1–7

[9] Lozano, J.G., Cadaval, E.R.: 'Battery equalization active methods', *J. Power Sources*, 2014, **246**, pp. 934–949

[10] Lindemark, B.: 'Individual cell voltage equalizers (ICE) for reliable battery performance'. Proc. IEEE 13th Int. Telecommunications Energy Conf., Kyoto, Japan, November 1991, pp. 196–201

[11] Nishijima, K., Sakamoto, H., Harada, K.: 'A PWM controlled simple and high performance battery balancing system'. Proc. IEEE Power Electronics Specialists Conf., Galway, Ireland, June 2000, vol. 1, pp. 517–520

[12] Cassani, P.A., Williamson, S.S.: 'Design testing and validation of a simplified control scheme for a novel plug-in hybrid electric vehicle battery cell equalizer', *IEEE Trans. Ind. Electron.*, 2010, **57**, (12), pp. 3956–3962

[13] Phung, T., Collet, A., Crebier, J.C.: 'An optimized topology for next-to-next balancing of series-connected lithium-ion cells', *IEEE Trans. Power Electron.*, 2014, **26**, (9), pp. 4603–4613

[14] Mestrallet, F., Kerachev, L., Crebier, J.-C., *et al.*: 'Multiphase interleaved converter for lithium battery active balancing', *IEEE Trans. Power Electron.*, 2014, **29**, (6), pp. 2874–2881

[15] Zou, C., Zhou, C., Zhang, L.: 'Estimation of cell SOC evolution and system performance in module-based battery charge equalization systems', *IEEE Trans. Smart Grid*, 2018, pp. 1–1, DOI: 10.1109/TSG.2018.2867017

[16] Li, X., Xu, J., Xu, S., *et al.*: 'Two-switch equaliser for series-connected battery stack using zeta type converter and symmetrical capacitor–diode circuit', *Electron. Lett.*, 2017, **53**, pp. 1600–1602

[17] Fang, Y.H., Hua, C.C., Chuang, C.W.: 'Low-cost switched capacitor charge equaliser with cancellation mechanism of alternating current', *IET Power Electron.*, 2016, **9**, (7), pp. 1454–1461

[18] Baughman, A.C., Ferdowsi, M.: 'Double-tiered switched-capacitor battery charge equalization technique', *IEEE Trans. Ind. Electron.*, 2008, **55**, (6), pp. 2277–2285

[19] Yuanmao, Y., Cheng, K.W.E., Yeung, Y.P.B.: 'Zero-current switching switched-capacitor zero-voltage-gap automatic equalization system for series battery string', *IEEE Trans. Power Electron.*, 2012, **27**, (7), pp. 3234–3242

[20] Kim, M., Kim, C., Kim, J., *et al.*: 'A chain structure of switched capacitor for improved cell balancing speed of lithium-ion batteries', *IEEE Trans. Ind. Electron.*, 2014, **61**, (8), pp. 3989–3999

[21] Park, H.S., Kim, C.E., Kim, C.H., *et al.*: 'A modularized charge equalizer for an HEV lithium-ion battery string', *IEEE Trans. Ind. Electron.*, 2009, **56**, (5), pp. 1464–1476

[22] Hoque, M.M., Hannan, M.A., Mohamed, A.: 'Optimal algorithms for the charge equalisation controller of series connected lithium-ion battery cells in electric vehicle applications', *IET Electr. Syst. Transp.*, 2017, **7**, (4), pp. 267–277

[23] Kutkut, N.H.: 'A modular non dissipative current diverter for EV battery charge equalization'. Proc. 13th Annual IEEE Applied Power Electronics Conf. Exposition, Anaheim, CA, USA, February 1998, pp. 686–690

[24] Chen, Y., Liu, X., Cui, Y., *et al.*: 'A multi-winding transformer cell-to-cell active equalization method for lithium-ion batteries with reduced number of driving circuits', *IEEE Trans. Power Electron.*, 2019, **31**, (7), pp. 4916–4929

[25] Park, S.H., Park, K.B., Kim, H.S., *et al.*: 'Single-magnetic cell-to-cell charge equalization converter with reduced number of transformer windings', *IEEE Trans. Power Electron.*, 2012, **27**, (6), pp. 2900–2911

[26] Hua, C.-C., Fang, Y.-H., Li, P.-H.: 'Charge equalisation for series-connected $LiFePO_4$ battery strings', *IET Power Electron.*, 2015, **8**, (6), pp. 1017–1025

[27] Lim, C.S., Lee, K.J., Ku, N.J., *et al.*: 'A modularized equalization method based on a magnetizing energy for series-connected lithium-ion battery string', *IEEE Trans. Power Electron.*, 2014, **29**, (4), pp. 1791–1799

[28] Li, S., Mi, C.C., Zhang, M.: 'A high-efficiency active battery-balancing circuit using multiwinding transformer', *IEEE Trans. Ind. Appl.*, 2013, **49**, (1), pp. 198–207

[29] Shang, Y., Xia, B., Zhang, C., *et al.*: 'An automatic equalizer based on forward-flyback converter for series-connected battery strings', *IEEE Trans. Ind. Electron.*, 2017, **64**, (7), pp. 5380–5391

[30] Uno, M., Kukita, A.: 'Bidirectional PWM converter integrating cell voltage equalizer using series-resonant voltage multiplier for series-connected energy storage cells', *IEEE Trans. Power Electron.*, 2015, **30**, (6), pp. 3077–3090

[31] Nguyen, T.T.N., Yoo, H.G., Oruganti, S.K., *et al.*: 'Neuro-fuzzy controller for battery equalisation in serially connected lithium battery pack', *IET Power Electron.*, 2015, **8**, (3), pp. 458–466

[32] Chen, H., Zhang, L., Han, Y.: 'System-theoretic analysis of a class of battery equalization systems: mathematical modeling and performance evaluation', *IEEE Trans. Veh. Technol.*, 2015, **64**, (4), pp. 1445–1457

[33] Han, W., Zhang, L., Han, Y.: 'Mathematical modeling, performance analysis and control of battery equalization systems: review and recent developments', in Li, J., Zhou, S., Han, Y. (Eds.): '*Advances in battery manufacturing, services, and management systems*' (Wiley-IEEE Press, USA, 2016, 1st edn.), pp. 281–301

[34] Ju, F., Deng, W., Li, J.: 'Performance evaluation of modularized global equalization system for lithium-ion battery packs', *IEEE Trans. Autom. Sci. Eng.*, 2017, **13**, (2), pp. 986–996

[35] Xiong, R., Cao, J.Y., Yu, Q.Q., *et al.*: 'Critical review on the battery state of charge estimation methods for electric vehicles', *IEEE Access*, 2017, **6**, pp. 1832–1843

[36] Hageman, S.C.: 'Using PSpice to simulate the discharge behavior of common batteries', *MicroSim Appl. Notes*, 1996, p. 291

8 Appendix

$m - n$ is rewritten as

$$\begin{aligned} m - n &= \frac{a(aR_0 - 1 - 2kR_0)}{(aR_0 - 1)((aR_0 - 1) - 2kR_0)C} \\ &= \frac{a}{(aR_0 - 1)C} \\ &= \frac{1}{(R_0 - 2R)C} < 0. \end{aligned} \tag{29}$$

$m + n$ is rewritten as

$$\begin{aligned} m + n &= \frac{2k + a(aR_0 - 1 - 2kR_0)}{(aR_0 - 1)((aR_0 - 1) - 2kR_0)C} \\ &= \frac{(a - 2k)(aR_0 - 1)}{(aR_0 - 1)((aR_0 - 1) - 2kR_0)C} \\ &= -\frac{-\left((TR(1 + B) - 4L(1 - B))/2TR^2(1 + B)\right)}{((aR_0 - 1) - 2kR_0)C}. \end{aligned} \tag{30}$$

As $((aR_0 - 1) - 2kR_0)C < 0$, the key is to prove that $-((TR(1 + B) - 4L(1 - B))/2TR^2(1 + B))$ is less than zero. It is assumed that

$$f\left(x=\frac{TR}{L}\right)=-\frac{TR(1+B)-4L(1-B)}{2TR^2C(1+B)}$$
$$=\frac{4L(1-\mathrm{e}^{-RT/(2L)})-TR(1+\mathrm{e}^{-RT/(2L)})}{2TR^2C(1+\mathrm{e}^{-RT/(2L)})} \quad (31)$$
$$=\frac{4(1-\mathrm{e}^{-x/2})-x(1+\mathrm{e}^{-x/2})}{2xRC(1+\mathrm{e}^{-x/2})}$$

Then, the key is to prove that $f(x)$ is less than zero. Because x is always greater than zero, we only need to prove $f_1(x)=4(1-\mathrm{e}^{-x/2})-x(1+\mathrm{e}^{-x/2})$ is less than zero when $x>0$. The first and the second derivatives of $f_1(x)$ are

$$f_1'(x)=-1+\mathrm{e}^{-x/2}+\frac{1}{2}x\,\mathrm{e}^{-x/2} \quad (32)$$

$$f_1''(x)=-\frac{1}{4}x\,\mathrm{e}^{-x/2}. \quad (33)$$

Due to $x>0$, $f_1''(x)<0$. So $f_1'(x)$ is a monotonically decreasing function. Hence, $f_1'(x)<f_1'(x\to 0)=0$, and $f_1(x)<f_1(x\to 0)=0$ is obtained.